The N2D Haptic Glove: A Multi-Finger Glove for 2D Directional Force Feedback for Contact Rich Manipulation

Authors Redacted

Abstract— Humans rely on directional fingertip forces to probe and regulate contact during manipulation, yet most wearable haptic gloves render only vibration or single-axis force, leaving force direction ambiguous. Without directional cues, users must infer contact force from vision alone, often leading to over-pressing, inconsistent control, and reduced precision in robotic teleoperation. We present the N2D Haptic Glove, a multi-finger wearable device that renders planar flexion-extension fingertip forces using capstan-drive transmissions for high-transparency force feedback. Through benchtop validations and a user study involving haptic teleoperation of a robotic arm and hand, we demonstrate that compared to visual-only and single-axis haptic baselines, planar fingertip feedback significantly reduces contact force error during precise manipulation, improves trial-to-trial consistency, and enhances overall user experience in axial probing tasks. These findings establish the N2D Haptic Glove and directional finger-based haptics devices as a promising modality for contact-rich teleoperation, immersive virtual reality simulations, and robot learning from demonstrations.

I. INTRODUCTION

Haptic devices have been widely utilized in immersive contexts, ranging from interacting with virtual reality (VR) environments to teleoperating robotic surgical systems for minimally invasive surgery. Recent interest in using human demonstrations to train robot imitation learning policies requires human teleoperators to control manipulators within real or virtual worlds, where haptic feedback has been shown to collect tighter and more informed distributions of trajectories [1].

With the rise of the humanoid form factor for robotics, a key challenge has been developing effective control methods for robotic hands. While recent VR-based teleoperation systems enable dexterous control through visual feedback [2], the absence of haptic cues limits operators' ability to regulate contact forces and avoid errors [3]. To address this, existing haptic gloves provide cable-driven flexion resistance [4–6] and fingertip-mounted cutaneous feedback [7, 8].

Directional haptic rendering in finger interactions remains underdeveloped. In this work, we define *transverse* forces as those aligned with finger flexion/extension at the finger pad, and *axial* forces as those acting along the length of the finger, such as during poking. Consider moving a finger through a cluttered set of objects: the perception of axial forces at the finger tip can be just as vital — if not more so — than transverse forces generated along the closing grasping direction. Accurate perception of both is essential for contact-rich manipulation tasks, including probing, gentle grasping, and slip detection.
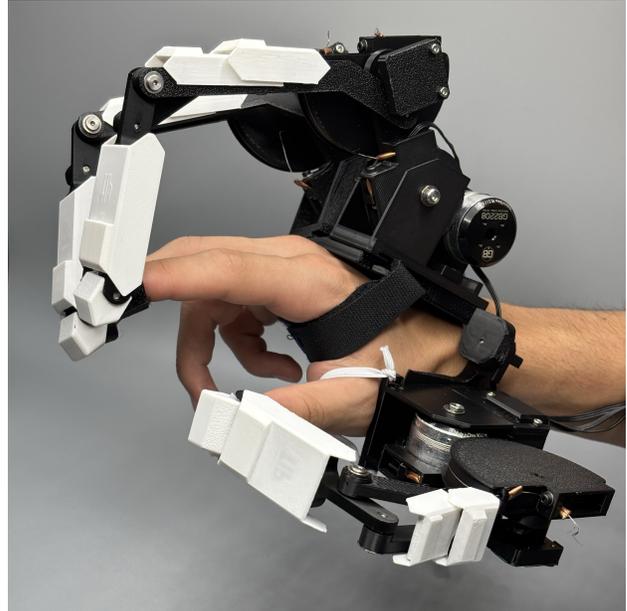

Fig. 1: **The N2D Haptic Glove:** is the first, multi-fingered glove design that offers 2D force feedback along the axial direction of multiple fingers. The glove provides multi-directional haptic rendering, an integral feedback capability for tasks requiring probing, gentle grasping, slip detection, etc., which rely on directional forces.

A current indirect approach to approximate directional feedback is to use skin-shear on a held device [9], [10]; however, delivering axial force feedback directly to individual fingertips is arguably more natural and interpretable.

In this paper, we present the first wearable haptic interface with on-hand actuation capable of rendering planar kinesthetic forces at multiple finger tips (Fig. 1). Named the N2D Haptic Glove — for N fingers and 2D force rendering per finger — doubling the DOF per finger of active force-feedback over existing designs, with applications in robot teleoperation, VR simulations, and imitation learning.

The key novel contributions of this paper are as follows:

1) The first multi-fingered haptic glove capable of delivering planar force feedback to the finger,
2) Design of the N2D Haptic Glove to achieve high transparency through low-friction, zero-backlash transmissions for clean, accurate haptic rendering,
3) Validation of 2D planar directional feedback ability with benchtop testing, and
4) Demonstrating the benefits of N2D Haptic Glove's directional haptics in a teleoperation user study.

TABLE I: Comparison of Fingertip-Feedback Systems

#	Feature	SenseGlove R1	HaptGlove	DOGlove	NURing	Fluid Reality	AirPush	N2D Glove
1	Multi-DOF Fingertip Forces	✗	✗	✗	✓	✗	✓	✓
2	Kinesthetic Force Feedback	✓	✓	✓	✓	✗	✗	✓
3	Multi-Digit (simultaneous)	✓	✓	✓	✗	✓	✗	✓

II. RELATED WORKS

In the realm of fingertip haptics, existing wearable interfaces can be grouped by the combination of features they support: multi-DOF fingertip forces, kinesthetic force feedback, and multi-digit actuation.

Several devices render controllable force directions at the fingertip but are generally limited to single-finger designs. Skin-stretch devices generate tangential cues through multi-directional deformation of the fingerpad [7], [11], [12]. AirPush demonstrates multi-directional fingertip forces using compressed air with 2-DOF control [13]. Similarly, the NURing delivers two-dimensional kinesthetic deflection cues via tendon-driven actuation on the index finger [14]. These designs achieve directional rendering but cannot scale to multi-finger use cases such as dexterous grasping.

A second class of devices provides feedback across multiple fingers but is limited to cutaneous stimulation without kinesthetic force. Vibrotactile actuators simulate contact events and palpation cues through fingertip-mounted vibration pads [15], [16]. Fluid Reality achieves high-resolution pressure rendering across five fingertips using pump arrays [17]. These approaches offer rich tactile information but cannot reproduce the sustained, directional forces needed for precise manipulation.

Several integrated glove systems target multi-finger kinesthetic feedback. SenseGlove R1 delivers four-finger resistance through an active force-feedback exoskeleton [6]. Dexmo provides multi-digit resistive feedback through a link-bar exoskeleton [18]. DOGlove provides five-finger active force feedback augmented with vibrotactile sensing at a low cost [5]. HaptGlove combines pneumatic clutches with skin indenters across all five fingers [19]. While each system delivers active kinesthetic force feedback across multiple fingers, all restrict fingertip forces to a single axis without directional rendering.

Collectively, these systems represent significant progress across individual dimensions of haptic feedback, but none combine directional fingertip forces, kinesthetic resistance, and multi-digit coverage in a single device. The N2D Haptic Glove addresses this gap (Table I).

III. METHODS

The following sections describe: (A) the mechanical design of the N2D Haptic Glove linkage system, (B) the electromechanical framework, (C) kinematic analysis of the glove, and (D) a 2D planar haptic feedback rendering approach for multi-fingered force reflectance.
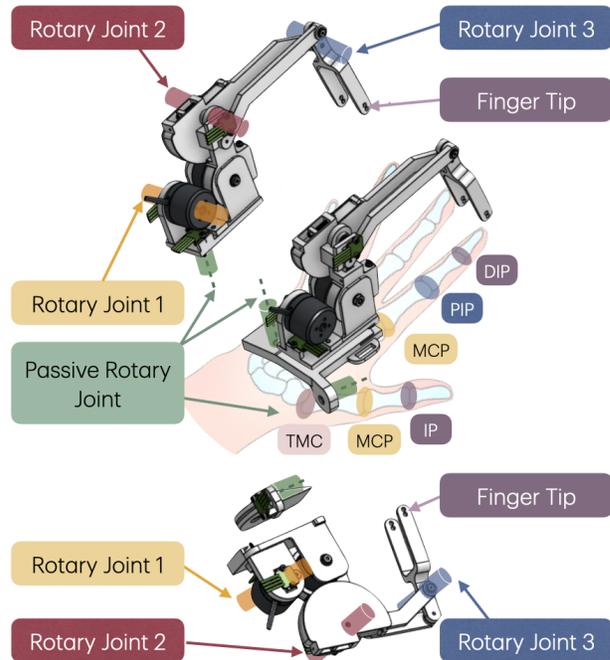

Fig. 2: Deconstructed view of the N2D Haptic Glove showing finger linkage joint layout and its correspondence to hand anatomy.

A. Mechanical Design Overview

The N2D Haptic Glove is designed to preserve the natural biomechanical DOFs of the hand. Following established models [20], the MCP joint is treated as a saddle joint allowing flexion-extension and adduction-abduction, while the PIP and DIP joints are modeled as revolute joints constrained to flexion-extension. The thumb additionally performs opposition at the TMC joint. The thumb, index, and middle fingers are central to most grasping and probing tasks due to their roles in precision and stability.

The device consists of three modular finger subsystems mounted along a structural backbone. Each subsystem uses a crossed four-bar linkage with an additional link to permit full flexion-extension while enabling 2D planar force feedback. Planar fingertip forces are generated by actuating the proximal links via capstan cable drives (see Kinematic Modeling). Each linkage is mounted on a passive rotary joint for finger abduction-adduction, with the thumb having an additional passive joint for TMC opposition. The resulting 2-DOF planar formulation provides physiologically grounded kinematics while enabling controlled directional force feedback at each fingertip (Fig. 2), consistent with validated models of lateral pinch [21].

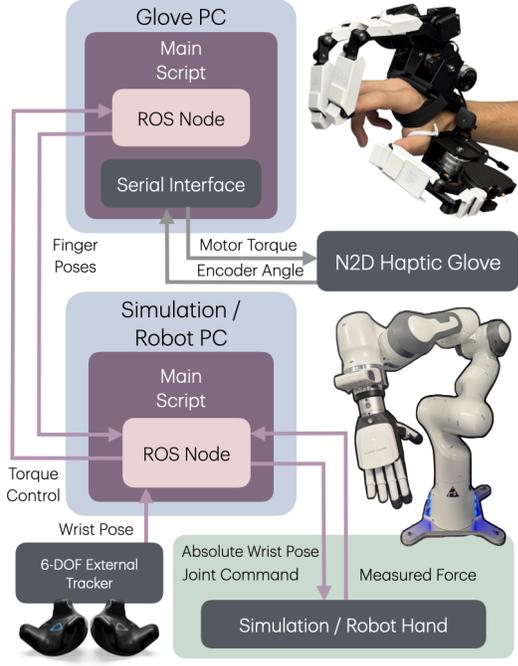Beyond directional force feedback, the glove prioritizes

Fig. 3: System architecture of the N2D Haptic Glove. The Glove PC computes finger poses from encoder data and sends joint commands to the Simulation/Robot PC via ROS. Sensed interaction forces are returned and mapped to motor commands.

haptic transparency. All active DOFs are actuated via capstan drives powered by brushless motors, avoiding geared transmissions that introduce backlash, friction, and damping. Actuators are mechanically grounded at the base of the linkage system, preventing motor masses from rotating about the finger joints and eliminating the sensation of actuator mass swinging on the finger. All transmissions remain on the hand, avoiding the resistance, hysteresis, and unmodeled dynamics introduced by off-hand routing such as Bowden cables or pneumatic hoses.

The N2D glove weighs 562 g, with a detailed breakdown provided in Table II; the battery is excluded, as it is off-hand. Nearly half of the total mass comes from PLA components, suggesting that reduced infill, structural redesign, and lighter materials could substantially decrease weight. The other major contribution comes from the gimbal motors, which is a notable design constraint. Future advances in gimbal motor miniaturization will also lower overall system mass.

B. Electromechanical Architecture

Fig. 3 summarizes the electromechanical architecture and distributed control enabling torque-transparent capstan-drive actuation in the N2D Haptic Glove. GB2208 gimbal motors were selected for their compact form factor and high-torque, low-speed output without planetary gearing. Six motors are powered by DRV8313 three-phase drivers from a 12 V supply, each paired with an AS5048B 14-bit absolute magnetic encoder for rotor angle feedback. Four additional AS5048B encoders measure the passive abduction–adduction joints.

TABLE II: Weight breakdown of the N2D Haptic Glove

Qty	Component	Unit Weight (g)	Total (g)
6	Gimbal Motor	39.5	237
6	Motor Driver	4.5	27
10	Encoder	1	10
1	Main PCB	14	14
—	PLA & COTS parts	274	274
	Total Weight:		**562**

Each motor–encoder pair interfaces with a Teensy 4.1 microcontroller running field-oriented control in torque mode at *1 kHz*, while higher-level torque commands are transmitted from the Glove PC at *10 Hz* over a serial connection.

On the Glove PC, a calibration script generates a user-specific profile of finger link lengths and 6-DOF finger poses. The main control script loads this profile and publishes hand state through a ROS node. An external VIVE Tracker 3.0 provides absolute wrist pose, which is fused with fingertip pose estimates. A corresponding ROS node on the robot side receives these poses and commands the robot arm and hand. Measured interaction forces are returned through ROS and mapped to torque commands for the glove, closing the bilateral control loop.

C. Kinematic Modeling

Each finger's kinematic model computes fingertip pose and force relative to its base joint. These are transformed into a unified hand frame, then into the world frame using the estimated hand pose, localizing each digit in the environment.

The device is modeled as a set of modular finger linkage subsystems mounted to a common base (Fig. 4). Each link is treated as a rigid body with orientation $\mathbf{R} \in SO(3)$ and position $\mathbf{p} \in \mathbb{R}^3$, and transformations between bodies are represented using homogeneous transforms:

$$\mathbf{T}_i^j = \begin{bmatrix} \mathbf{R}_i^j & \mathbf{p}_i^j \\ \mathbf{0}_{1\times3} & 1 \end{bmatrix} \quad (1)$$

which represents the pose of coordinate frame i expressed in coordinate frame j.

We define a canonical base frame for the device $\{base\}$ with fixed origin set at the position-tracker's origin and orientation. Each digit, $f \in \{T,I,M\}$ (Thumb, Index, Middle) has a constant finger base coordinate frame $\mathbf{T}_{T,base}^{base}, \mathbf{T}_{I,base}^{base}, \mathbf{T}_{M,base}^{base}$ described in the position-tracker origin.

For non-thumb fingers ($f = I,M$), the kinematics of the linkages from the finger's base $f,base$ to the tip can be described using three revolute joints $q_{f,0}, q_{f,1}, q_{f,2}$ and link lengths $a_{f,0}, a_{f,1}, a_{f,2}, a_{f,3}$. The distal tip pose $\{tip\}$ described in the base frame $\{base\}$ is

$$\mathbf{T}_{f,tip}^{f,base}(\mathbf{q}^f, \mathbf{a}^f, \mathbf{l}^f, \mathbf{p}^f) = \mathbf{T}_{f,0}^{f,base} \mathbf{T}_{f,1}^{f,0} \mathbf{T}_{f,2}^{f,1} \mathbf{T}_{f,3}^{f,2} \mathbf{T}_{f,tip}^{f,3} =$$
$$\begin{bmatrix} \mathbf{R}_y(q_{f,0}) & \mathbf{0}_{3\times1} \\ \mathbf{0}_{1\times3} & 1 \end{bmatrix} \begin{bmatrix} \mathbf{R}_z(q_{f,1}) & \mathbf{p}_{f,1}^0 \\ \mathbf{0}_{1\times3} & 1 \end{bmatrix}$$
$$\begin{bmatrix} \mathbf{R}_z(q_{f,2}) & \mathrm{tr}_x(a_{f,1}+l_5) \\ \mathbf{0}_{1\times3} & 1 \end{bmatrix} \begin{bmatrix} \mathbf{R}_z(q_{f,3}) & \mathrm{tr}_x(a_{f,2}) \\ \mathbf{0}_{1\times3} & 1 \end{bmatrix}$$
$$\begin{bmatrix} \mathbf{I}_{3\times3} & \mathrm{tr}_x(a_{f,3}) \\ \mathbf{0}_{1\times3} & 1 \end{bmatrix} \quad (2)$$
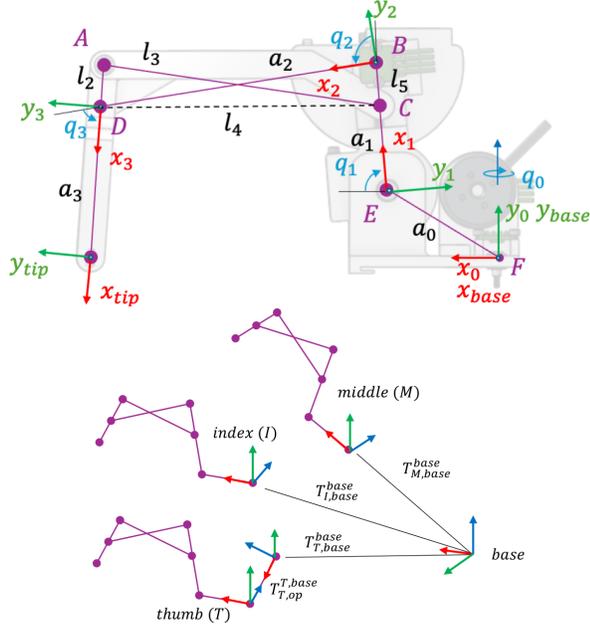
Fig. 4: Kinematic analysis of a finger linkage. (Top) Single finger linkage with three DOFs defined by $q0, q1, q2$ (with $q3$ being a driven joint by $q1$ and $q2$) is shown. (Bottom) Finger linkages on the glove body show the overall coordinate frames with extra passive DOF for thumb opposition.

where $\mathbf{R}_z$ is the 3×3 rotation matrix about z and $\mathbf{tr}_x(a_{(\cdot)}) = [a_{(\cdot)}, 0, 0]^\top$. Angle $q_{f,3}$ is driven by $q_{f,1}$ and $q_{f,2}$. We solve $q_{f,3}$ via the cosine law by first computing the diagonal CD, then the internal angles $\angle ADC$ and $\angle BDC$, and finally taking their difference. Such that

$$CD = l_4 = \sqrt{a_2^2 + l_5^2 + 2a_2 l_5 \cos q_{f,2}} \quad (3)$$

$$\angle ADC = \arccos\left(\frac{l_2^2 + l_4^2 - l_3^2}{2 l_2 l_4}\right) \quad (4)$$

$$\angle BDC = \arccos\left(\frac{l_4^2 + a_{f,2}^2 - l_5^2}{2 l_4 a_{f,2}}\right) \quad (5)$$

$$q_{f,3} = \angle ADC - \angle BDC \quad (6)$$

The resultant position of each finger in its base frame is

$$x_{f,tip}^{f,base} = c_0((\mathbf{p}_{f,1}^{f,0})_x + a_1 c_{123} + a_{f,2} c_{12} + (a_{f,1} + l_{f,5}) c_1) \quad (7)$$

$$y_{f,tip}^{f,base} = (\mathbf{p}_{f,1}^{f,0})_y + l_{f,2} s_{123} + a_{f,3} s_{12} + (a_{f,1} + l_{f,5}) s_1 \quad (8)$$

$$z_{f,tip}^{f,base} = -s_0((\mathbf{p}_{f,1}^{f,0})_x + a_1 c_{123} + a_{f,2} c_{12} + (a_{f,1} + l_{f,5}) c_1) \quad (9)$$

with shorthand notation used, e.g., $s_0 = \sin(q_{f,0})$ and $c_{123} = \cos(q_{f,1} + q_{f,2} + q_{f,3})$.

The thumb ($f = T$) has an additional passive joint providing affordance for opposition, with the modified transformation:

$$\mathbf{T}_{T,tip}^{T,base}(\mathbf{q}^T, \mathbf{a}^T) = \mathbf{T}_{T,op}^{T,base} \mathbf{T}_{T,0}^{T,op} \mathbf{T}_{T,1}^{T,0} \mathbf{T}_{T,2}^{T,1} \mathbf{T}_{T,3}^{T,2} \mathbf{T}_{T,tip}^{T,3} \quad (10)$$

where $\mathbf{T}_{T,op}^{T,base} = \begin{bmatrix} \mathbf{R}_z(q_{T,op}) & \mathbf{p}_{op}^{base} \\ \mathbf{0}_{1 \times 3} & 1 \end{bmatrix}$ describes the additional

link transform, and then $\mathbf{T}_{T,0}^{T,op} = \begin{bmatrix} \mathbf{R}_y(q_{T,0}) & \mathbf{0}_{3 \times 1} \\ \mathbf{0}_{1 \times 3} & 1 \end{bmatrix}$ followed

by the same transforms.

Given the pose of the glove in the world $\mathbf{T}_{base}^w$, as measured by an optical tracker, we can derive the pose (position and orientation) of each finger in the world via

$$\mathbf{T}_{f,tip}^w = \mathbf{T}_{base}^w \, \mathbf{T}_{f,base}^{base} \, \mathbf{T}_{f,tip}^{f,base} = \begin{bmatrix} \mathbf{R}_{f,tip}^w & \mathbf{p}_{f,tip}^w \\ \mathbf{0}_{1 \times 3} & 1 \end{bmatrix} \quad (11)$$

The finger tip positions ($f = \{T, I, M\}$) in the world are thus

$$\mathbf{p}_{f,tip}^w = \begin{bmatrix} x_{f,tip}^w & y_{f,tip}^w & z_{f,tip}^w \end{bmatrix}^\top \quad (12)$$

D. Multi-digit Haptic Rendering

Directional haptics are rendered by mapping Cartesian forces in the world frame, $\mathbf{f}_f^w \in \mathbb{R}^3$, to joint torques $\boldsymbol{\tau}_f \in \mathbb{R}^2$ via Jacobian transpose:

$$\boldsymbol{\tau}_f = \mathbf{J}_f^w(\mathbf{q}_f)^\top \mathbf{f}_f^w \quad (13)$$

where $\mathbf{J}_f^w(\mathbf{q}_f) = \begin{bmatrix} \frac{\partial \mathbf{p}_f^w}{\partial q_{f,1}}, \frac{\partial \mathbf{p}_f^w}{\partial q_{f,2}} \end{bmatrix} \in \mathbb{R}^{3 \times 2}$ is the Jacobian matrix of the position vector $\mathbf{p}_f^w$ w.r.t the joint angles $\mathbf{q}_f$. This formulation assumes quasi-static operation, neglecting link inertia and friction, as force transmission is geometry-dominated.

In teleoperation experiments, contact forces are measured directly as 3D Cartesian vectors in the world frame and applied without additional frame transformations. Only translational force components are rendered; moments and wrench relocation are not considered

Because each finger has only two active DOF, the set of achievable Cartesian forces lies in the column space of $\mathbf{J}_f^w(\mathbf{q}_f)$, whose columns correspond to the instantaneous Cartesian force directions generated by the two motors and thus define a configuration-dependent 2D subspace of $\mathbb{R}^3$. Any desired force can be decomposed as

$$\mathbf{f}_f^w = \mathbf{f}_f^{w,proj} + \mathbf{f}_f^{w,\perp} \quad (14)$$

where $\mathbf{f}_f^{w,proj} \in \mathrm{col}(\mathbf{J}_f^w)$ and $\mathbf{f}_f^{w,\perp} \in \mathrm{null}(\mathbf{J}_f^{w\top})$. Since $\mathbf{J}_f^{w\top} \mathbf{f}_f^{w,\perp} = 0$, this Jacobian transpose mapping eliminates the component out-of the plane, and the device implicitly renders the desired force onto its achievable 2D force subspace. The uncontrolled direction, corresponding to finger adduction and abduction, is therefore not reflected.

IV. EXPERIMENTS AND RESULTS

We conducted benchtop validation experiments along with a teleoperation user study to provide both quantitative and qualitative assessments of the N2D Haptic Glove, demonstrating its performance in controlled force rendering tasks as well as its effectiveness in real-world robotic teleoperation.

A. Validation Experiments

1) Planar Joint Actuation Experiment: A voltage–torque mapping for each joint is identified through a quasi-static directional calibration procedure. Motor torque is proportional to current; at the low velocities considered, back-EMF is negligible, allowing current to be approximated from applied voltage and internal motor resistance via Ohm's law.
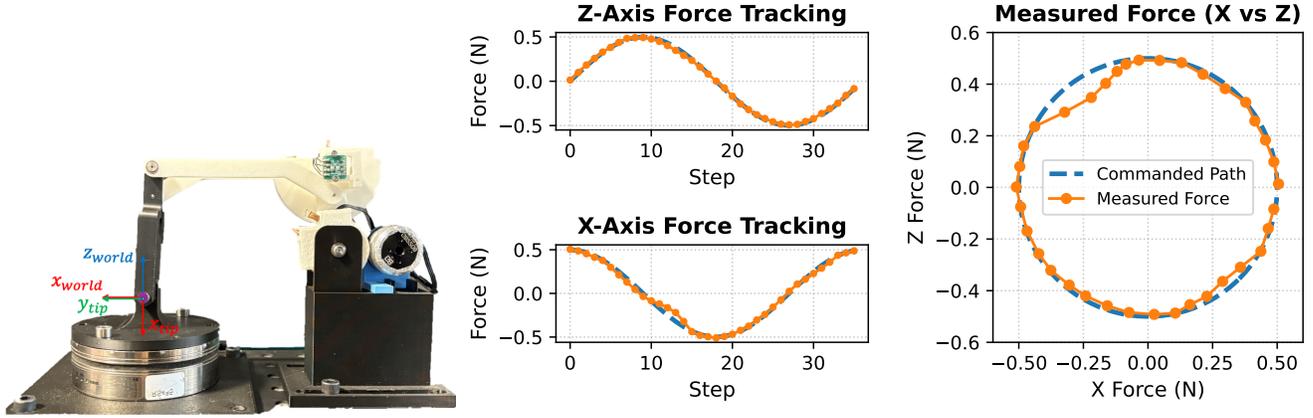
Fig. 5: Experimental force tracking results. (Left) Force calibration setup showing the world coordinate frame (x_{world}, z_{world}) and tip coordinate frame (x_{tip}, y_{tip}). (Center) Individual commanded and measured force components along the x and z axes. (Right) Measured forces plotted in the x–z plane compared to the commanded circular trajectory.

Planar fingertip forces are measured using an ATI Axia80 3-DOF force sensor. The finger linkage system was mounted at a chosen configuration where the finger tip coordinate axes coincides with the force sensor's measurement axes, as shown in Fig. 5. All commanded and measured forces are expressed in the world frame defined in the setup.

Joint torque is modeled as a voltage-dependent mapping

$$\tau_f = \begin{bmatrix} \zeta_1 f_{\text{poly}}(v_{f,1}, \mathbf{k}_{f,1}) & 0 \\ 0 & \zeta_2 f_{\text{poly}}(v_{f,2}, \mathbf{k}_{f,2}) \end{bmatrix} \quad (15)$$

where ζ_i are capstan gear ratios and $\mathbf{k}_{f,i}$ are polynomial coefficients. Using voltage sweeps $\mathbf{v}_f$ and measured Cartesian forces $\mathbf{f}_f^w$, the coefficients are solved in closed form via least squares using the Jacobian transpose relation in Eq. 13. Each finger is calibrated once.

To evaluate tracking accuracy, circular planar force trajectories were commanded. Figure 5 shows the commanded and measured force components f_x and f_z per step.

Force tracking performance is summarized by the root-mean-squared errors (RMSE): $\text{RMSE}_x = 0.032$ N, $\text{RMSE}_z = 0.014$ N, $\text{RMSE}_{|e|} = 0.034$ N, and $\text{RMSE}_\theta = 2.81°$. The commanded and measured force trajectories show close agreement in both magnitude and direction.

The fingertip Jacobian $\mathbf{J}_f^w$ is well-conditioned with $\kappa(\mathbf{J}_f^w) \approx 2.93$, indicating moderate directional sensitivity in torque-to-force transmission. The Jacobian remains full rank across all evaluated configurations, confirming that independent force components can be generated along both planar axes. These results demonstrate that forces can be rendered accurately throughout the x–z plane with minimal distortion.

Residual error is attributed to unmodeled nonlinearities in the voltage-torque mapping, particularly along directions where both motor axes contribute near-equally and commanded voltages are low, entering dead-zone regions. Capstan friction and motor saturation effects further contribute to magnitude and angular discrepancies.

2) Directional Force Generation Capability Analysis: To ensure the N2D Haptic Glove remains effective across different hand configurations, its ability to generate planar forces throughout the workspace must be evaluated. The workspace is defined here as the range of finger configurations achievable while wearing the glove. To characterize planar directional force capability across these configurations, we compute the manipulability index.

$$w(\mathbf{q}_f) = \sqrt{\det(\mathbf{J}_{\mathbf{f},\mathbf{xz}}^{\mathbf{w}}(\mathbf{q_f})\mathbf{J}_{\mathbf{f},\mathbf{xz}}^{\mathbf{w}}{}^\top(\mathbf{q_f}))} = \left|\det(\mathbf{J}_{\mathbf{f},\mathbf{xz}}^{\mathbf{w}}(\mathbf{q_f}))\right| \quad (16)$$

for all achievable configurations, where $\mathbf{J}_{\mathbf{f},\mathbf{xz}}^{\mathbf{w}}(\mathbf{q_f}) \in \mathbb{R}^{2\times 2}$ is the planar fingertip Jacobian obtained from the x-z rows of the full Jacobian. The value w is a scalar metric that quantifies the system's ability to generate planar forces in multiple directions at a given configuration. Higher values indicate more uniform and effective directional force generation, whereas $w(\mathbf{q}_f) \to 0$ indicates proximity to a singular configuration and reduced force controllability.

Fig. 6 shows the resulting manipulability color maps for two participants representing small and large hand sizes (15.4 cm and 20.5 cm hand length, respectively, within reported adult ranges [22]). To obtain the configuration space, participants performed maximal flexion, extension, abduction, and adduction movements.

After normalization, 58% of sampled configurations have manipulability values at or above 0.82. The configuration used in the planar joint actuation experiment also has normalized manipulability 0.82, indicating that over half of the sampled workspace is at least as well conditioned for planar force generation as the experimentally validated configuration. This result suggests that the glove can provide effective directional force output across a broad range of reachable finger postures, rather than only near a small set of favorable configurations for different hand sizes.

3) Haptic Teleoperation with Franka Arm Experiment: Although seemingly simple, pushing is fundamental to manipulation, particularly for probing and confirming discrete contacts such as button presses. In teleoperated settings—e.g., operating control panels or medical equipment—pushing becomes difficult without appropriate haptic
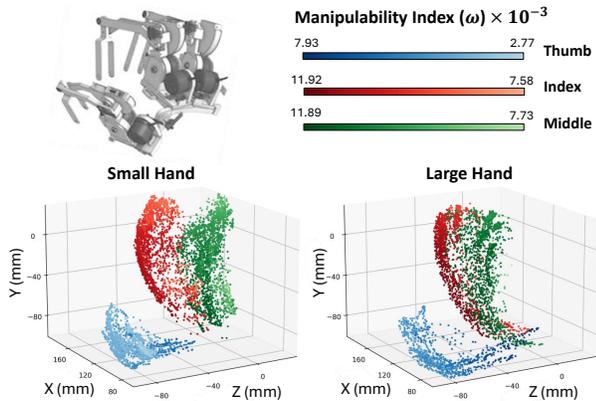
Fig. 6: Workspace range of motion for a small and large hand (scatter points). The overlaid manipulability colormap indicates configuration-dependent directional force capability, showing well-conditioned force generation throughout typical operating regions.

feedback. Vision alone cannot reliably confirm contact when visual motion is minimal, and 1D force feedback fails to capture off-axis interactions. Thus, accurate multi-DOF force feedback is essential for natural execution of pushing tasks.

To evaluate the glove's ability to render realistic forces during pushing, we conducted a user study simulating teleoperated button pressing. Participants teleoperated a Franka Emika Panda robot equipped with an RH56DFTP dexterous hand with tactile sensing array to press on a digital scale toward a target weight while wearing the N2D Haptic Glove. Three feedback conditions were tested: no haptics, 1D haptics (one motor disabled to emulate a 1-DOF resistive tendon glove), and full 2D haptics.

In all conditions, participants received visual feedback via a live video stream of the robot hand and scale to limit depth cues. The scale display was hidden to replicate typical VR and teleoperation constraints.

All participants pressed the scale to a target weight under all three haptic modes across four conditions defined by finger contact orientation and target weight, with group order quasi-randomized. Contact orientation included axial probing (finger tip contact) and transverse probing (finger pad contact), while target weight was set to 50 g or 100 g, yielding four condition combinations.

Before each condition and haptic mode, participants completed a 2-minute training period with the corresponding feedback active to calibrate visual and force perception. During training, the scale display was visible. Afterward, participants performed five trials in which they pressed the scale—by lowering their hand—to what they perceived as the target weight. The true scale reading was recorded for each trial by the study organizer.

Performance was evaluated by the absolute error between the true scale weight and the target weight. Furthermore, users completed two NASA-TLX [23] surveys afterwards, one for each finger contact location experience.

A total of 16 participants completed the user study, with Figure 8 showing the absolute error boxplot distribution and
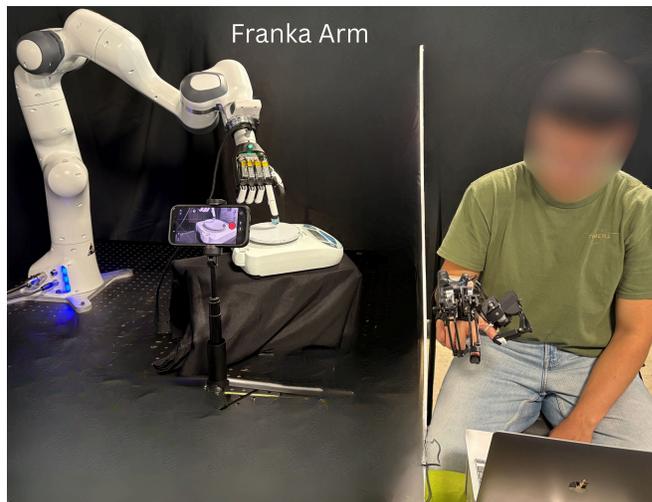

Fig. 7: Franka Arm and Inspire Hand scale pressing task setup. Participants teleoperated the robot to press a digital scale toward a target weight under three feedback conditions: no haptics, 1D haptics, and 2D haptics.

Table III presenting the statistical analysis of all four groups across haptic feedback modes.

To evaluate whether haptic feedback modality, target weight, and finger contact location statistically affect absolute error from target, a linear mixed-effects model (LMM) was used. Absolute error was treated as the dependent variable, with haptic modality, target weight, and contact location as fixed effects. Additionally, participant was included as a random intercept to account for participant baseline differences and the experiment's repeated-measures structure.

An LMM was chosen, as opposed to Friedman or Kruskal-Wallis with post-hoc tests, due to non-independence of repeated measurements from a participant across trials and groups. Therefore, an LMM allows all individual trial data to be retained while appropriately accounting for within-participant correlations, maintaining statistical power. Planned pairwise contrasts between haptic feedback modalities were performed using Holm-corrected p-values to control for multiple comparisons, with the significance level chosen as $\alpha = 0.05$.

In axial probing conditions, median absolute error decreased progressively from no haptic to 1D to 2D feedback, indicating improved accuracy with higher-fidelity force rendering. The LMM results corroborate this trend: at the 100 g target, 2D feedback significantly outperformed both 1D and no-feedback conditions, with large estimated differences favoring 2D. These findings demonstrate that 2D haptic feedback significantly enhances force regulation and precision during axial interactions, where single-DOF resistive tendon feedback is insufficient.

At the 50 g target, the reduction in median error from 1D to 2D was not statistically significant, likely because 50 g approaches the lower bound of the motors' effective operating range. Notably, 2D feedback produced more consistent performance, reflected by a smaller interquartile range of

TABLE III: Per-trial absolute error statistics across target weight and contact conditions ($n = 16$ participants). Median absolute errors (g) per condition decreases with more degrees of haptic feedback for all groups. *p*-values are from planned pairwise contrasts of a linear mixed-effects model with Holm correction. Negative estimated differences indicate reduced error relative to the comparison modality. From these results, 2D haptic feedback generally yields significantly less error.

| Group	Mode	Median Abs Err (Q1–Q3) (g)	*p* (vs Vis)	Est. Diff vs Vis (g)	*p* (vs 1D)	Est. Diff vs 1D (g)
Axial 50g	Visual	37.68 (20.20-63.00)	–	–	2.53×10^{-4}	+39.40
	1D	30.80 (12.28-50.00)	2.53×10^{-4}	−39.40	–	–
	2D	24.99 (11.25-38.23)	2.56×10^{-6}	−50.60	0.276	−11.20
Axial 100g	Visual	50.25 (29.88-93.91)	–	–	0.032	+26.18
	1D	34.73 (10.00-87.45)	0.032	−26.18	–	–
	2D	21.20 (9.20-43.63)	1.43×10^{-5}	−55.27	0.032	−29.09
Transverse 50g	Visual	42.52 (25.00-88.25)	–	–	4.09×10^{-4}	+36.43
	1D	27.65 (14.53-50.00)	4.09×10^{-4}	−36.43	–	–
	2D	27.85 (13.24-47.43)	5.07×10^{-4}	−34.94	0.876	+1.49
Transverse 100g	Visual	89.30 (57.00-179.08)	–	–	0.0315	+49.02
	1D	61.00 (27.10-116.59)	0.0315	−49.02	–	–
	2D	46.52 (15.88-113.25)	0.0315	−49.40	0.985	−0.37
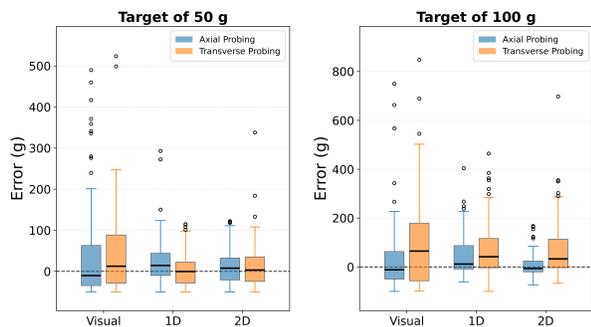
Fig. 8: Boxplots of absolute error (g) for target weights of 50 g and 100 g. In axial probing, median error decreases progressively from visual-only to 1D to 2D feedback. In transverse probing, both 1D and 2D feedback reduce error compared to visual-only, with no significant difference between 1D and 2D.
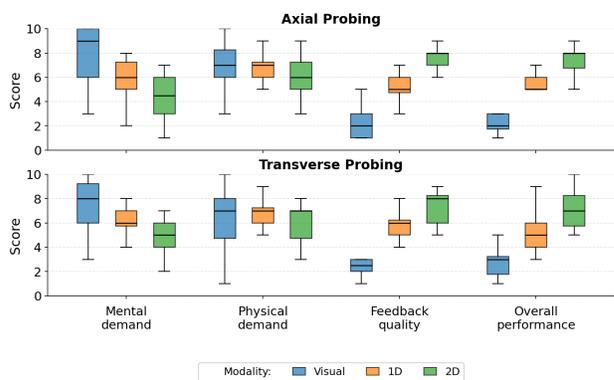

Fig. 9: Individual NASA TLX survey results for axial probing and transverse probing, demonstrating multi-directional haptic feedback significantly reduces cognitive load while improving overall performance for participants.

absolute error compared to visual-only and 1D conditions.

In transverse probing conditions, participants performed significantly better with either 1D or 2D haptic feedback compared to no feedback. However, no statistically significant difference was observed between the 1D and 2D modes, with an estimated effect size near zero. These results suggest that the presence of directional force feedback—regardless of dimensionality—is sufficient to improve accuracy and reduce error during transverse interactions, while 2D feedback offers no measurable advantage over 1D. This outcome is expected, as transverse probing forces can be effectively rendered using conventional 1-DOF resistive tendon-based gloves.

Subjective feedback further reinforces the value of the N2D Haptic glove over existing 1D resistive tendon gloves. NASA TLX ratings indicate that when receiving 2D haptic feedback for both axial and transverse probing, participants expressed that their perceived performance increased with more control and clearer feedback, while their mental demand decreased, as seen in Figure 9. Moreover, responses indicate total perceived physical demand only decreased marginally with 2D haptic feedback due to the excessive weight of the glove present for all three feedback modes, as

expressed by multiple participants.

Taken together, results from our study show that planar force feedback enhances both objective force regulation and subjective user experience in teleoperated tasks.

V. DISCUSSIONS AND CONCLUSIONS

Directional fingertip haptics are essential for realistic physical interaction in teleoperation. We presented the design, analysis, validation, and user study of the N2D Haptic Glove to evaluate the impact of multi-directional feedback.

Results show that 2D haptic feedback significantly improves precision in axial probing and pressing tasks by reducing force error and increasing consistency. This highlights the feasibility of implementing the N2D haptic glove for VR and teleoperation axial probing tasks, such as pushing small buttons or searching a confined medical environment for surgical tools with finger tips.

Although effectiveness of the N2D Haptic Glove for transverse probing is comparable to 1D haptic feedback, the collective results suggest the glove will still enable more precise manipulation than existing 1D haptic gloves for tasks in between full axial and full transverse probing directions.

Additionally, N2D Haptic Glove's 2-DOF force feedback improves user experience and confidence, further proving its value for teleoperation and VR simulation tasks.

Collectively, these findings demonstrate that multi-directional force feedback allows users to regulate contact forces more accurately and consistently across a broader range of tasks. The N2D Haptic Glove thus provides a foundation for next-generation wearable haptic interfaces that support more natural and effective human–robot interaction.

Although the work demonstrates accurate multi-directional force rendering, several limitations remain. The current design actuates three fingers and weighs 562 g; scaling to all five would increase total mass to approximately 780 g. At the current weight, the glove can become fatiguing during extended use, despite the GB2208 being one of the best torque-to-weight motors on the market. Another limiting factor is the deadzone at the lower bound of the motor's operating voltage, which limits feedback for very precise, low-force tasks. Ongoing advances in drone motor technology are rapidly improving motor size and efficiency, which is likely to reduce these constraints and offer a more effective N3D option in the future.

In conclusion, the N2D Haptic Glove demonstrates that multi-directional haptics are both feasible and beneficial for contact-rich tasks, particularly those involving axial probing. Our user study highlights its advantage in fingertip button pressing, but similar benefits extend to tasks categorized as peg-in-hole insertion, where sensing lateral misalignment forces can substantially improve guidance and task completion time. More broadly, the N2D Haptic Glove may be integrated with immersive simulation environments [24, 25], used in medical teleoperation systems [26], and incorporated into imitation learning pipelines [27]. These applications demonstrate the value of multi-directional fingertip feedback as a missing modality in current wearable haptic systems.

REFERENCES

[1] C. Cuan, A. Okamura, and M. Khansari, "Leveraging haptic feedback to improve data quality and quantity for deep imitation learning models," *IEEE Transactions on Haptics*, vol. 17, no. 4, pp. 984–991, 2024.

[2] X. Cheng, J. Li, S. Yang, G. Yang, and X. Wang, "Open-TeleVision: Teleoperation with immersive active visual feedback," in *Conference on Robot Learning (CoRL)*, 2024.

[3] V. Nitsch and B. Färber, "A meta-analysis of the effects of haptic interfaces on task performance with teleoperation systems," *IEEE Transactions on Haptics*, vol. 6, no. 4, pp. 387–398, 2013.

[4] S. Baik, S. Park, and J. Park, "Haptic glove using tendon-driven soft robotic mechanism," *Frontiers in bioengineering and biotechnology*, vol. 8, p. 541105, 2020.

[5] H. Zhang, S. Hu, Z. Yuan, and H. Xu, "DOGlove: Dexterous manipulation with a low-cost open-source haptic force feedback glove," *arXiv preprint arXiv:2502.07730*, 2025.

[6] SenseGlove B.V., "SenseGlove R1." https://www.senseglove.com/project-rembrandt/, 2025. Accessed: 2025.

[7] D. Trinitatova and D. Tsetserukou, "FiDTouch: A 3D wearable haptic display for the finger pad," *arXiv preprint arXiv:2507.07661*, 2025.

[8] HaptX Inc., "HaptX gloves G1." https://haptx.com/gloves-g1/, 2025. Accessed: 2025.

[9] S. B. Schorr, Z. F. Quek, I. Nisky, W. R. Provancher, and A. M. Oka-mura, "Tactor-induced skin stretch as a sensory substitution method in teleoperated palpation," *IEEE Transactions on Human-Machine Systems*, vol. 45, no. 6, pp. 714–726, 2015.

[10] L. T. Gwilliam, A. J. Doxon, and W. R. Provancher, "Haptic matching of directional force and skin stretch feedback cues," in *2013 World Haptics Conference (WHC)*, pp. 19–24, IEEE, 2013.

[11] Z. F. Quek, S. B. Schorr, I. Nisky, W. R. Provancher, and A. M. Okamura, "Sensory substitution and augmentation using 3-degree-of-freedom skin deformation feedback," *IEEE Transactions on Haptics*, vol. 8, no. 2, pp. 209–221, 2015.

[12] J. Min, S. Jang, S. Lee, and Y. Cha, "Ultralight soft wearable haptic interface with shear-normal-vibration feedback," *Advanced Intelligent Systems*, p. 2500374, 2025.

[13] Y. Ma, T. Xie, P. Zhang, H. Kim, and S. Je, "Airpush: A pneumatic wearable haptic device providing multi-dimensional force feedback on a fingertip," in *Proceedings of the 2024 CHI Conference on Human Factors in Computing Systems*, pp. 1–13, 2024.

[14] T. P. Trzpit, G. Reardon, A. Shilati, E. M. Gerber, M. A. Peshkin, and J. E. Colgate, "NURing: A tendon-driven wearable ring for on-demand kinesthetic haptic feedback," in *IEEE World Haptics Conference (WHC)*, 2025.

[15] H. Kim, H. Yi, H. Lee, and W. Lee, "HapCube: A wearable tactile device to provide tangential and normal pseudo-force feedback on a fingertip," in *Proceedings of the 2018 CHI Conference on Human Factors in Computing Systems*, pp. 1–13, 2018.

[16] C. Pacchierotti, D. Prattichizzo, and K. J. Kuchenbecker, "Cutaneous feedback of fingertip deformation and vibration for palpation in robotic surgery," *IEEE Transactions on Biomedical Engineering*, vol. 63, no. 2, pp. 278–287, 2016.

[17] V. Shen, T. Rae-Grant, J. Mullenbach, C. Harrison, and C. Shultz, "Fluid reality: High-resolution, untethered haptic gloves using electroosmotic pump arrays," in *Proceedings of the 36th Annual ACM Symposium on User Interface Software and Tech.*, pp. 1–20, 2023.

[18] X. Gu, Y. Zhang, W. Sun, Y. Bian, D. Zhou, and P. O. Kristensson, "Dexmo: An inexpensive and lightweight mechanical exoskeleton for motion capture and force feedback in vr," in *Proc. of the 2016 CHI Conf. on Human Factors in Computing Systems*, pp. 1991–1995, 2016.

[19] J. Qi, F. Gao, G. Sun, J. C. Yeo, and C. T. Lim, "HaptGlove—untethered pneumatic glove for multimode haptic feedback in reality–virtuality continuum," *Advanced Science*, vol. 10, no. 25, p. 2301044, 2023.

[20] K. S. Fok and S. M. Chou, "Development of a finger biomechanical model and its considerations," *Journal of biomechanics*, vol. 43, no. 4, pp. 701–713, 2010.

[21] A. Lemos, L. Rodrigues da Silva, B. Nagy, P. Barroso, and C. Vimieiro, "Biomechanical hand model: Modeling and simulating the lateral pinch movement," *Experimental Mechanics*, vol. 64, no. 9, pp. 1557–1578, 2024.

[22] C. C. Gordon, T. Churchill, C. E. Clauser, B. Bradtmiller, J. T. McConville, I. Tebbetts, and R. A. Walker, "1988 anthropometric survey of u.s. army personnel: Summary statistics (interim report)," Tech. Rep. ADA209600, U.S. Army Natick Research, Development and Engineering Center, Natick, MA, 1989.

[23] S. G. Hart, "Nasa-task load index (nasa-tlx); 20 years later," in *Proceedings of the human factors and ergonomics society annual meeting*, vol. 50, pp. 904–908, Sage publications Sage CA: Los Angeles, CA, 2006.

[24] A. Gani, O. Pickering, C. Ellis, O. Sabri, and P. Pucher, "Impact of haptic feedback on surgical training outcomes: a randomised controlled trial of haptic versus non-haptic immersive virtual reality training," *Annals of Medicine and Surgery*, vol. 83, p. 104734, 2022.

[25] K. Li, S. M. Wagh, N. Sharma, S. Bhadani, W. Chen, C. Liu, and P. Kormushev, "Haptic-ACT: Bridging human intuition with compliant robotic manipulation via immersive VR," *arXiv preprint arXiv:2409.11925*, 2024.

[26] X. Guo, F. McFall, P. Jiang, J. Liu, N. Lepora, and D. Zhang, "A lightweight and affordable wearable haptic controller for robot-assisted microsurgery," *Sensors*, vol. 24, no. 9, p. 2676, 2024.

[27] K. Li, D. Chappell, and N. Rojas, "Immersive demonstrations are the key to imitation learning," in *IEEE International Conference on Robotics and Automation (ICRA)*, pp. 5071–5077, 2023.